scientific reports

Check for updates

OPEN

Using ECG-derived respiration for explaining BOLD-fMRI fluctuations during rest and respiratory modulations

Inês Esteves[1]✉, Ana R. Fouto[1,2], Amparo Ruiz-Tagle[1,3], Gina Caetano[1] & Patrícia Figueiredo[1]

Recording physiological signals during fMRI is valuable for multiple purposes but often requires additional setup, increasing complexity and participant discomfort. This is particularly challenging in simultaneous EEG-fMRI studies, which typically already include electrocardiogram (ECG) recordings. Here, we aim to leverage the known modulation of ECG by respiration to obtain an ECG-derived respiration (EDR) signal without extra equipment. We acquired EEG-fMRI data from 15 healthy subjects during resting state and two respiratory challenges (slow-paced breathing and breath-holding), with simultaneous ECG and respiratory recordings. Multiple methods were used to extract EDR signals, and the results were evaluated by comparing them with recorded respiration and assessing the quality of physiological regressors for denoising and cerebrovascular reactivity estimation. Amplitude-based EDR methods showed lower correlations with respiration, likely due to ECG distortion in the MRI. Nevertheless, coherence analysis showed that EDR preserved the relevant spectral content. EDR-based regressors were similar to those obtained from measured respiration. Notably, a method based on heart rate variability performed best overall, yielding physiological noise correction and reactivity estimates comparable to those using recorded respiration. Our results demonstrate that meaningful respiratory information can be extracted from ECG within the MRI environment, benefiting EEG-fMRI studies when respiration cannot be reliably recorded.

Keywords Functional magnetic resonance imaging (fMRI), Respiration, Electrocardiogram (ECG), ECG-derived respiration (EDR), Resting state, Respiratory fluctuation

Functional magnetic resonance imaging (fMRI) indirectly assesses brain activity by measuring changes in the blood-oxygen level dependent (BOLD) signal, allowing the mapping of brain regions involved in task-induced activation or functionally connected. Since the BOLD contrast relies on hemodynamic changes, which are also influenced by physiological processes such as cardiac pulsatility and respiration, these may represent confounds when interpreting the BOLD signal[1–4]. Physiological signal acquisition during fMRI may serve multiple purposes: modeling and correction of non-neuronal BOLD sources, study of physiological modulations of brain activity, or simply monitoring physiological states throughout experiments[5]. Although there are some fMRI data-driven methods used for physiological denoising (e.g. CompCor[6]; FMRIB's ICA-based X-noiseifier (FIX)[7]; ICA-based Automatic Removal Of Motion Artifacts (ICA-AROMA)[8], most methods rely on measuring cardiac and respiratory signals. Critically, this requires additional setup, as for example direct measurement of respiration typically relies on MR-compatible devices such as respiratory belts (tracking chest or abdominal expansion) or capnography (measuring exhaled CO_2)[5,9]. While these approaches provide accurate respiratory signals, they increase experimental complexity, prolong preparation times, and may heighten subject discomfort or motion artifacts, particularly in long or multimodal protocols such as EEG-fMRI[9].

Respiration is known to modulate the electrocardiogram (ECG), affecting the morphology of the heartbeats[10], altering the electrical impedance of the thoracic cavity due to filling/emptying of the lungs[11], and affecting the heart rate[12]. Consequently, it is possible to obtain an ECG-derived respiration (EDR) signal[13]. Methods for EDR estimation have been widely explored in the context of ambulatory care[14,15], but only one previous EEG-fMRI study reported the use of EDRs in the MRI environment[16]. Importantly, in EEG-fMRI experiments, which are becoming increasingly common, placing a single-lead ECG on the back is already standard practice

[1]ISR-Lisboa/LARSyS and Department of Bioengineering, Instituto Superior Técnico, Universidade de Lisboa, Lisbon, Portugal. [2] Algarve Biomedical Center, Universidade do Algarve, Faro, Portugal. [3] Faculdade de Ciências da Saúde, Universidade Europeia, Lisbon, Portugal. ✉email: ines.esteves@edu.ulisboa.pt

for *a posteriori* correction of the pulse artifact induced on the EEG[17]. Thus, the ECG is typically available in these setups, making EDR estimation possible without additional preparation, extra MR-compatible devices, or increased subject discomfort[16]. Compared with conventional respiratory measures, EDR may provide a practical surrogate of respiration that captures physiologically meaningful variability in the BOLD signal, while avoiding the logistical and technical challenges of extra equipment. This makes EDR particularly promising when dedicated respiratory recordings are not available, the signal is corrupted, or in retrospective analyses of existing datasets. The study by Abreu et al. (2017) compared the use of a subject-specific physiological model derived from several EDRs with an image-based physiological model (based on cerebrospinal fluid (CSF) and white matter (WM) average time courses) and with FIX[7,16]. The data corrected using the physiological model achieved the best performance in terms of sensitivity and specificity to map epileptic networks and the default mode network. Unfortunately, the MRI environment introduces distortions in the ECG wave morphology as a consequence of both magnetic induction due to movements inside the main magnetic field as well as the effects of radiofrequency pulses[18]. Because the respiratory data were not recorded in that study to provide a ground-truth for comparison with the EDR, it remains to be validated whether EDRs in the MRI environment can be robustly obtained.

In this work, we aim to fill this gap in the literature by evaluating EDR signals obtained during EEG-fMRI acquisitions. For this purpose, we collected EEG-fMRI data including simultaneous ECG and respiration recordings, from healthy participants during resting state and while they performed two respiratory challenges aimed at modulating respiration patterns: a slow-paced breathing task and a breath-holding task. We considered these tasks to test the ability of EDR to capture such respiratory variations, which are commonly utilized to assess cerebrovascular reactivity (CVR)[19]. We compared EDR signals with the measured respiratory signals, by assessing their similarity in time and frequency (correlation and coherence) and their ability to predict physiological contributions in fMRI signals, both for physiological denoising and CVR mapping.

Materials and methods

Data acquisition

Data were acquired in the context of a larger research project on brain imaging in migraine (MigN2Treat), taking place at Hospital da Luz, Lisboa. The methods and results corresponding to the other MRI protocols are described elsewhere[20–26]. The research protocol and statistical analysis were not preregistered. All methods were performed in accordance with the relevant guidelines and regulations. The study was approved by the Hospital da Luz Ethics Committee and all participants provided written informed consent according to the Declaration of Helsinki 7th revision.

Sample

Data was acquired from 15 female healthy subjects (age: median = 30, IQR = 10.5). The participants were healthy, without any diagnosed condition that significantly impaired an active and productive life or reduced their life expectancy to be below 5 years. None of them was undergoing treatment with psychoactive drugs, including anxiolytics, antidepressants, anti-epileptics, or any migraine prophylactics. Furthermore, being pregnant or having contraindications for MRI scanning (e.g. claustrophobia, pacemaker, incompatible implants) were also exclusion criteria.

MRI data

The MRI data acquisition was performed with a 3T Siemens Vida system, using a 64-channel RF coil. Functional T2*-weighted images were obtained using 2D-Echo Planar Imaging (EPI), TR/TE = 1260/30ms, flip angle = 70º, in-plane generalized autocalibrating partially parallel acquisition (GRAPPA) acceleration factor of 2, simultaneous multi-slice (SMS) with a factor of 3, 60 slices, with 2.2 mm isotropic resolution. Structural T1-weighted images were acquired with a magnetization-prepared rapid gradient echo (MPRAGE) sequence, with TR = 2300 ms, TE = 2.98 ms, inversion time (TI) = 900 ms, and 1 mm isotropic resolution. Field map magnitude and phase images were obtained using a double-echo gradient echo sequence (TR = 400.0 ms, TE = 4.92/7.38 ms, voxel size: 3.4 × 3.4 × 3, flip angle 60∘).

Physiological data

The respiratory signal was continuously recorded with the integrated BioMatrix Sensors from Siemens, through Siemens Physiological Monitoring Unit (PMU), with a sampling frequency of 400 Hz. The ECG was acquired simultaneously with fMRI as part of the MR-compatible BrainAmp MR EEG system (Brain Products), with a sampling frequency of 5000 Hz, using an Ag/AgCl ring-type electrode placed on the back as caudally as possible, on the left of the spine. The impedance was maintained below 25 kOhm. The SyncBox was used to ensure synchronization between the MRI scanner clock (10 MHz) and the BrainAmp MR system, to improve the quality of the gradient artifact (GA) correction.

Tasks

EEG-fMRI data was acquired during resting state (RS) and two respiratory tasks involving respiratory modulations, slow-paced breathing (SPB) and breath-holding (BH). Due to technical issues, some respiratory recordings had missing values at the start or end. These signals were excluded from the analysis and were therefore not included in our sample sizes, except for RS. Consequently, not all tasks were analyzed for every subject, with only a subgroup of participants considered for each task. For RS, we retained the maximum amount of available data that still provided a reasonable duration. Although the original task lasted 7 min, only 4.82 min (229 fMRI volumes) per subject were usable for analysis. During RS ($N = 10$), subjects were instructed to keep their eyes open, looking at a black screen, without thinking of anything in particular. The SPB task ($N = 9$)

consisted of an initial fixation cross (5 s), a 1-min free breathing period, a 2-min 0.1 Hz paced respiration with visual written instructions for inhaling (5 s) and exhaling (5 s), and another 1-min free breathing period (194 fMRI volumes). The BH task ($N = 12$) comprised 4 cycles of post-exhalation breath-hold (15 s) followed by free breathing and naturally paced breathing, with a total of approximately 4.47 min (213 fMRI volumes). The natural breathing frequency of each subject was computed beforehand based on a calibration recording performed outside the scanner, during a period longer than 1 min while the subject was not performing any particular task. The median breathing period was 4 s for all task sub-samples, ranging from 3 to 4 s for RS, and 3–5 s for BH and SPB sub-samples. For each subject, all tasks were performed on the same day. The timings of each task are depicted in Fig. 1.

Data analysis

The fMRI data was preprocessed using FMRIB Software Library (FSL) tools[27]. MATLAB version 2016b was used for respiration and ECG data preprocessing as well as further analysis and visualization. The data analysis pipeline is shown in Fig. 2.

Data preprocessing

fMRI EPI distortion correction was performed using FMRIB's Utility for Geometrically Unwarping EPIs (FUGUE), to correct for geometric distortions and signal loss, using a fieldmap acquisition to characterize B_0 field inhomogeneities, containing magnitude and phase information. The Brain Extraction Tool (BET) was used to remove non-brain tissue. Volume realignment was performed by applying FMRIB's Linear Image Registration Tool (FLIRT) with respect to the middle volume, using 6 rigid body motion parameters (MP). Motion outliers (MO) were obtained using FSL Motion Outliers tool, with the dvars option, which considers the root mean square intensity difference of volume N to volume $N+1$, thresholded at the 75th percentile + 1.5 times the inter-quartile range (Power et al. 2012). High-pass temporal filtering with a cut-off frequency of 0.01 Hz was applied to remove slow drift fluctuations and spatial smoothing was performed using SUSAN tool (S.M. Smith and J.M. Brady, 1997), employing a Gaussian kernel with a full width half maximum of 3.3 mm for RS and 3.5 mm for SPB and BH. The code used for fMRI preprocessing can be accessed here: https://github.com/martaxavier/fMRI-Preprocessing.

The structural image was used to obtain a gray matter (GM) mask for the functional images. For that, following non-brain tissue removal, tissue segmentation was performed with FMRIB's Automated Segmentation Tool (FAST) to obtain GM partial volume effect (PVE) images, which were then thresholded, binarized and transformed to the subject's functional space using a registration matrix to the structural image obtained by applying FSL's FLIRT with 12 degrees of freedom.

Respiration Respiratory data (Resp) was matched with the fMRI acquisition, downsampled to 250 Hz and bandpass filtered from 0.01 to 1 Hz using a Butterworth filter of order 2. Peak detection was performed to find maximum and minimum values of inspiration and expiration, using a threshold based on the 80th percentile of the data for RS and BH, and on the 40th percentile for the SPB, since the amplitude of the signal during slow breathing was larger. This procedure was followed by manual verification and the threshold was readjusted to the 75th percentile for one subject.

ECG The ECG was corrected for the GA using the average artifact subtraction (AAS) method[28], implemented in the FMRIB plugin of the EEGLAB toolbox, using windows with 30 volumes and without performing adaptive noise cancelation, to avoid distorting the ECG waveform. The signal was then downsampled to 250 Hz and ECG R-peaks were automatically detected using a long short term memory (LSTM) network trained on ECG data acquired in the MR environment (https://github.com/LaSEEB/deepQRS) and manually inspected and corrected using an interactive tool (https://github.com/LaSEEB/interactiveQRS). Furthermore, we corrected for missing and false heart beats, using the approach proposed by de Chazal et al. (2003)[29], which had also been employed by Varon et al. (2020) prior to EDR computation[15]. This procedure resulted in the detection and correction of a

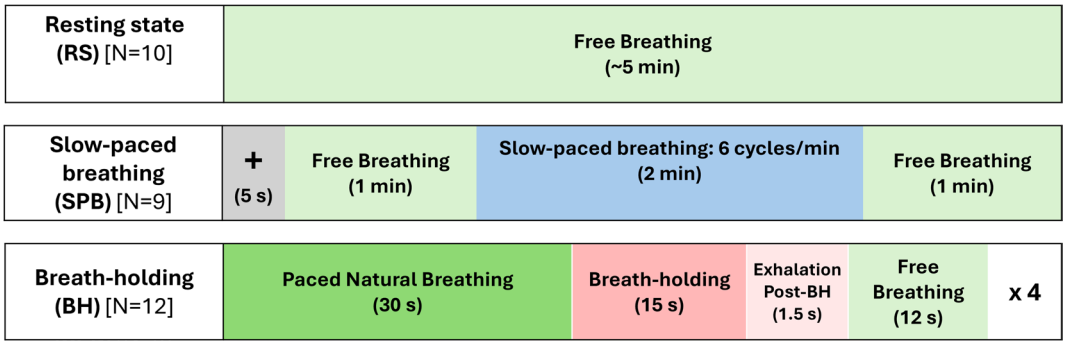

Fig. 1. Schematic representation of task timings for resting state (RS) and the two respiratory modulations, slow-paced breathing (SPB) and breath-holding (BH). Each task is divided into distinct intervals marked along the horizontal axis indicating the corresponding breathing pattern.

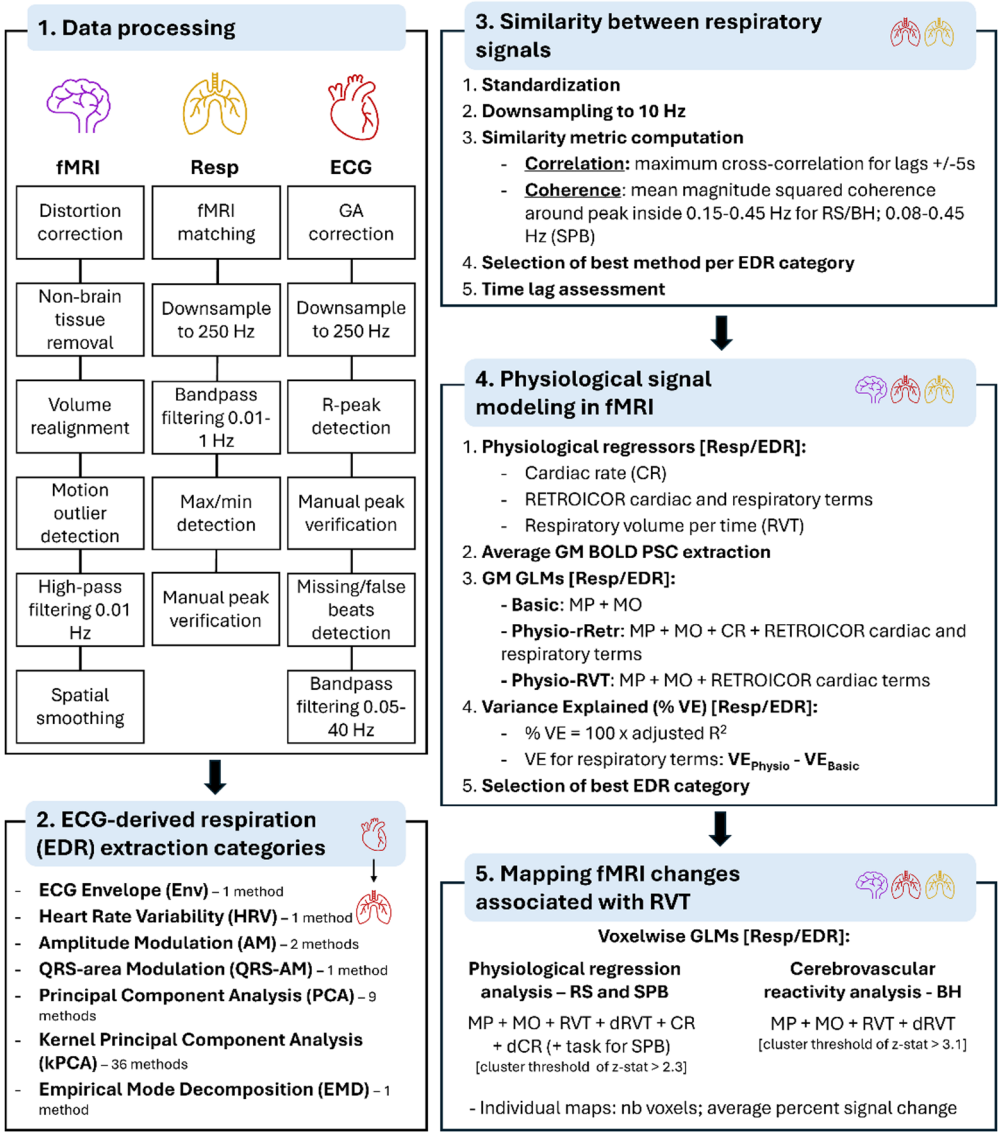

Fig. 2. Data analysis pipeline. *BOLD* blood oxygen level dependent, *CR* cardiac rate, *dCR* cardiac rate derivative, *dRVT* respiratory volume per time derivative, *GLM* general linear model, *GM* gray matter, *MP* motion parameters, *MO* motion outliers, *RVT* respiratory volume per time, *VE* variance explained.

missing peak for one subject, for the BH task. Finally, the signal was bandpass filtered 0.05–40 Hz using a FIR filter with a Hamming window. The lower edge of the band was chosen considering the preservation of respiratory frequencies.

ECG-derived respiration (EDR) extraction categories

EDRs were extracted using a publicly available repository (https://github.com/rmabreu/Respiratory_Signal_Estimation) which comprises methods from 7 categories: ECG envelope (ENV), heart-rate variability (HRV), amplitude modulation (AM), QRS-area modulation (QRS-AM), principal component analysis (PCA), kernel PCA (kPCA), and empirical mode decomposition (EMD), previously described in the work by Abreu et al. (2017). Each method leverages different ECG features with some focusing on amplitude (e.g., ENV, AM, QRS-AM), others on frequency components (e.g., HRV, EMD), and some using statistical decomposition techniques (e.g., PCA, kPCA). Several EDRs were obtained for AM, PCA and kPCA (e.g. variations relying on different ECG features, such as using either the whole beat or only the QRS or T wave portions), resulting in 51 EDRs per task for each subject. Some of the methods induced a steep rise/decrease of the EDR signal at the start or end, due to insufficient information for an accurate respiratory estimate. To correct abnormal fluctuations at the signal edges, we applied nearest-value interpolation if the absolute gradient in the first or last second exceeded 80% of the maximum absolute gradient of the entire signal. Peak detection of minimum and maximum values was performed using the same procedure that had been employed for respiratory signals.

Similarity between respiratory signals

We assessed the similarity between Resp and EDR signals in both the time and frequency domains, using correlation and coherence, respectively. To compute the similarity metrics for each participant and task, both signals were first standardized (mean of zero and standard deviation of one) and downsampled to 10 Hz[30,31]. Correlation was computed as the maximum cross correlation coefficient over a lag of +/-5s, optimizing for phase delays, and with no lag, to mimic a real situation with unknown optimal lags. Coherence was based on the magnitude squared coherence, estimated using Welch's method to obtain the spectra (1024-point Fast Fourier Transform; Hamming window; 8 segments with equal length and 50% of overlap). The mean magnitude squared coherence was computed for a range around the fundamental respiratory frequency (fR), considered to be the frequency with highest power within 0.15–0.45 Hz for RS and BH, and within 0.08–0.45 Hz for SPB. The range was determined by the frequencies around fR with more than half of the peak power[30,31].

For each category, we identified the EDR method yielding the highest correlation with Resp (using the optimal lag) for each task. The EDR method selected for each category was then identified based on a majority vote across the three tasks. For AM, a version without baseline removal was chosen by consensus, being the highest across all tasks. Both for PCA and kPCA, methods using the first principal component and the whole ECG beat were chosen, respectively, having achieved the highest correlation for SPB and BH. For kPCA, the method also included a polynomial kernel of order 2.

To determine whether the correlations were significantly greater than zero, we conducted a Wilcoxon signed-rank test for each EDR category and task, applying the Benjamini-Hochberg procedure to control the false discovery rate (FDR) across multiple comparions. To evaluate differences between categories within each task, we used a Kruskal-Wallis test followed by post hoc pairwise comparisons using the Dunn test with Sidák correction to control the family wise error rate (FWER). The significance level was set as $\alpha = 0.05$.

Physiological signal modeling in fMRI

To explore the impact on the physiological noise correction, nuisance regressors regarding respiration and cardiac pulsatility were obtained (with no lag): retrospective image correction (RETROICOR) terms, respiratory volume per time (RVT) and cardiac rate (CR). For RETROICOR, the phases of respiratory and cardiac cycles at each fMRI volume acquisition were estimated. A Fourier series up to the second order was built from respiratory and cardiac terms, accounting for quasi periodic signal fluctuations[4]. RVT considers non-periodic signal fluctuations due to changes in the depth and rate of breathing[1]. The RVT timecourse was obtained from the respiratory peaks and troughs using the amplitude (difference between consecutive maximum and minimum) divided by the time period between them. The result was interpolated to obtain a uniform sampling frequency corresponding to that of the fMRI, normalized and convolved with the respiratory response function as described by Birn et al. (2008)[2]. Similarly, for CR, the time difference between consecutive R peaks, which had been previously detected, was used to obtain the heart rate. The heart rate was interpolated, normalized and convolved with the cardiac response function as described in[3]. The respiratory regressors were estimated from EDRs and Resp, in this case without considering a lag.

The GM BOLD percent signal change (PSC) was calculated by first averaging the BOLD time series across all voxels within the GM mask to obtain a mean time course. The mean of this time course was then subtracted from each time point, and the result was divided by the same mean before being multiplied by 100. Three general linear models (GLM) were fitted to the GM BOLD PSC: Basic (6 MP, variable number of MO and, only for SPB, a task block convolved with the double-gamma hemodynamic response function (HRF)); Physio-rRetr (RETROICOR cardiac terms; CR; RETROICOR respiratory terms); and Physio-RVT (RETROICOR cardiac terms; CR; RVT). The two GLM's including respiratory regressors were estimated using either EDR or Resp for subsequent comparison. The variance explained (%VE) for each GLM was computed as 100 x adjusted R^2 (R^2_{adj}), and the %VE by the physiological terms was then obtained as (VE_{Physio}-VE_{Basic}) for Physio-rRetr and Physio-RVT.

As previously, we conducted a Wilcoxon signed-rank test for each EDR category and task to assess whether the variance explained was significantly greater than zero, applying the Benjamini-Hochberg procedure to control the FDR. In this case, respiration was also included in the comparison alongside the EDR categories. To evaluate differences among categories and compare them with Resp within each task, we used a Kruskal-Wallis test followed by post-hoc pairwise comparisons corrected using the Dunn test with Sidák correction, to control FWER. The significance level was set as $\alpha = 0.05$.

Mapping fMRI changes associated with RVT

The BOLD changes associated with RVT were mapped by fitting a GLM for each task, using FEAT (FMRI Expert Analysis Tool) v6.00. For RS and SPB, we incorporated RVT and CR in the GLM, along with their respective derivatives as well as MP and MO, as nuisance regressors. For SPB, we also added the task paradigm convolved with a double-gamma HRF to the GLM as the regressor of interest. Two models were created for each subject, one using RVT derived from Resp and another using RVT derived from the EDR method selected in the previous analysis. A cluster threshold of z-stat > 2.3 and a cluster significance level p-value < 0.05 were applied to generate thresholded z-stat maps for RVT. For BH, we included RVT in the GLM, as well as its temporal derivative, as a regressor of interest, since it may be used as a proxy of $PetCO_2$ for CVR mapping[32]. We also included MP and MO in the GLM as nuisance regressors. In this case, the clustering threshold was increased to z-stat > 3.1 to enhance the significance of the results. For the three tasks, we examined the maps of BOLD changes associated with each regressor, assessing the number of voxels that survived the threshold as well as the average PSC across the whole brain, GM and WM. Differences between Resp and HRV were tested using a Wilcoxon rank-sum test, followed by the Benjamini-Hochberg procedure to control the FDR. The significance level was set as $\alpha = 0.05$.

Results

Similarity metrics

Results are presented only for the EDR methods yielding the highest correlation coefficients with Resp for each category. The results for all methods are presented in the Supplementary Material. The similarity metrics computed between the EDR signals and Resp across all subjects and tasks are presented in Fig. 3. We found that, using optimal lags, the correlation between Resp and EDRs is significantly larger than zero for all categories, for RS, SPB and BH. Among the methods, EMD consistently outperforms others, while AM performs significantly worse than at least one other method for all tasks. Notably, HRV is significantly outperformed by other methods for RS and BH, but for SPB it shows high values, significantly exceeding AM. At zero lag, the differences in correlation between EDR methods become more pronounced. PCA and EMD consistently show stronger correlations, while Env and HRV perform consistently worse than at least two other methods. In terms of coherence, amplitude-based methods consistently show the poorest performance across all tasks. For RS, the methods that are not based on the amplitude perform similarly among them, with only EMD outperforming QRS-AM (amplitude-based). For SPB, the Env and HRV methods significantly outperform the lowest-performing method, AM. For BH, more subjects exhibit low coherence values across all methods, with no significant differences among them.

In line with the previous results, the example in Fig. 4 shows that the EDR methods differ in their ability to accommodate breathing changes. EDR waveforms of some of the methods resemble respiration, though with amplitude differences and a time shift. Nevertheless, in general, their power spectra overlap the respiratory frequency band.

Furthermore, the differences obtained for correlations considering the optimal lag relative to lag zero may be explained by the large scattering of optimal time lags, which are also mostly not centered around zero, as shown in Fig. 5.

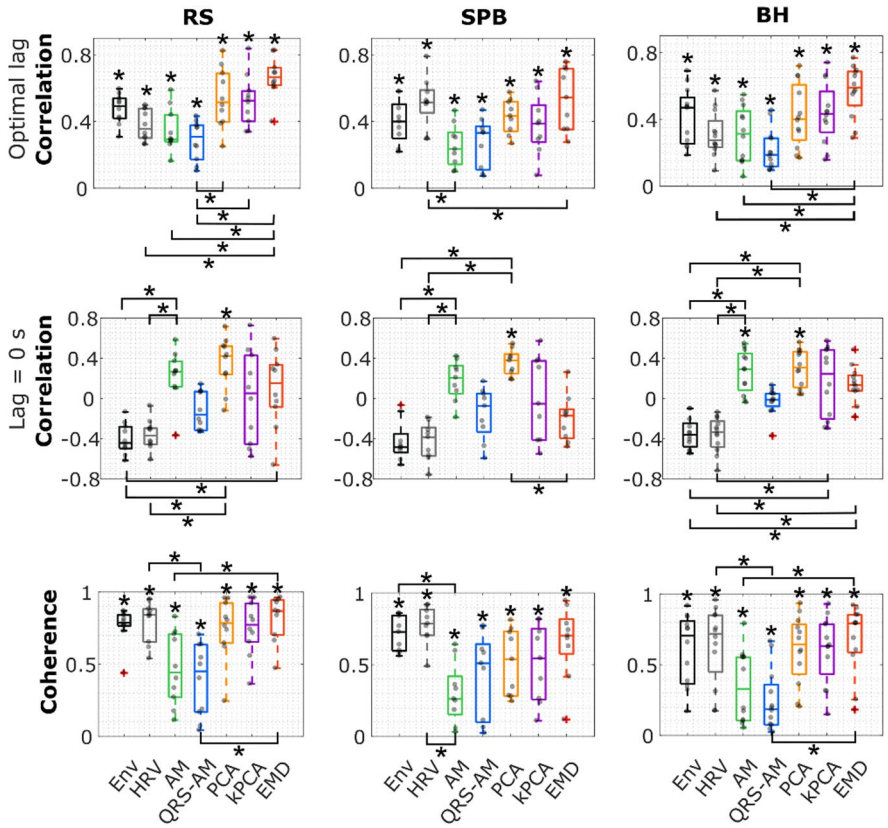

Fig. 3. Distributions across subjects of the similarity metrics between each EDR method and Resp (x-axis, colours): Correlation (Optimal lag: maximum cross-correlation over a lag = ± 5 s; No lag: correlation without at lag = 0 s); and Coherence. Square brackets with * outside the plots denote significant differences between methods (Kruskal-Wallis test, corrected p-values); * inside the plots denote values significantly larger than zero for each method (Wilcoxon signed-rank test, corrected p-values). *Env* ECG Envelope, *HRV* Heart Rate Variability, *AM* Amplitude Modulation, *QRS-AM* QRS-area Modulation, *PCA* Principal Component Analysis, *kPCA* Kernel Principal Component Analysis, *EMD* Empirical Mode Decomposition.

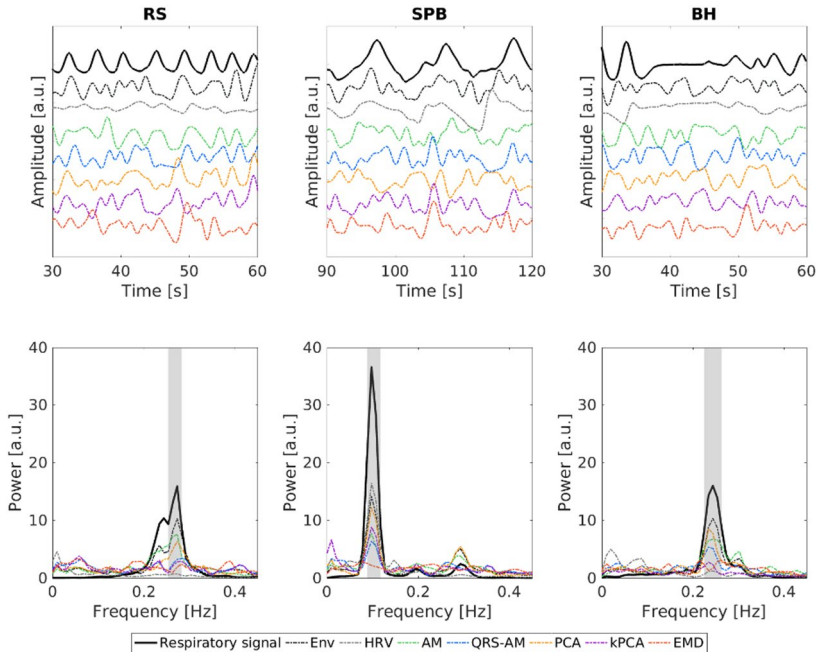

Fig. 4. Respiratory signals (black) and corresponding EDRs shifted by the optimal lag (colour), for the three tasks, in an illustrative subject: (Top) Signal amplitudes during a representative 30 s period of the task; and (Bottom) Power spectra for the whole signal (shaded area corresponds to the full width at half maximum of the power). The strong respiratory modulations in the SPB and BH tasks can be appreciated in the substantially different amplitude and spectral profiles. *Env* ECG Envelope, *HRV* Heart Rate Variability, *AM* Amplitude Modulation, *QRS-AM* QRS-area Modulation, *PCA* Principal Component Analysis, *kPCA* Kernel Principal Component Analysis, *EMD* Empirical Mode Decomposition.

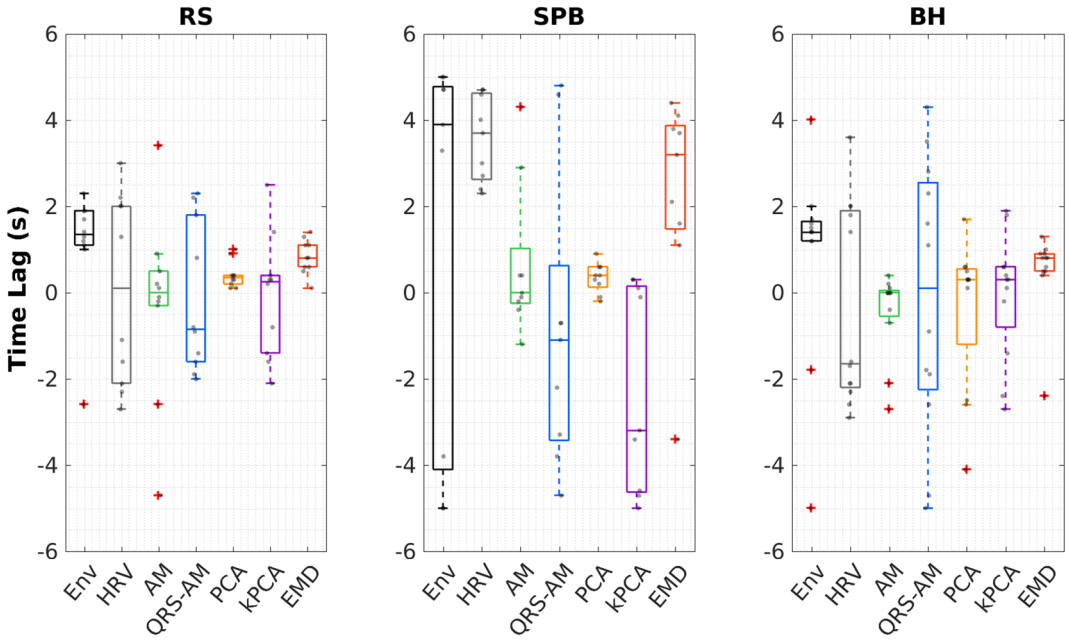

Fig. 5. Distributions across subjects of the time lag yielding the maximum correlation over a range of ± 5s between each EDR method and Resp (x-axis, colours), for each task. The scattering of optimal time lags varies across methods and is larger for the respiratory challenges, particularly SPB. *Env* ECG Envelope, *HRV* Heart Rate Variability, *AM* Amplitude Modulation, *QRS-AM* QRS-area Modulation, *PCA* Principal Component Analysis, *kPCA* Kernel Principal Component Analysis, *EMD* Empirical Mode Decomposition.

Physiological signal modelling in fMRI

Figure 6 depicts the average GM fMRI signal % VE by respiratory regressors (rRetr and RVT) computed based on Resp and the different EDR methods. The performance of EDRs for physiological regression of the BOLD signal differs for rRetr and RVT and is dependent on the task. Resp-based regressors only outperform the AM method, for the model including RVT for the BH task. In general, although smaller, the % VE by Resp is equivalent to the one explained by several EDR methods, with HRV method showing the best performance. Overall, results suggest that HRV is the most consistent method, particularly in the case of Physio-rRetr models. In general, the amplitude-based methods show the worst performance. For these reasons, the following analyses were performed only with HRV.

Figure 7 shows that the Basic and both Physio models (using Resp and HRV, the best performing EDR method) can fit the data, following it more closely in the case of respiratory tasks, as expected.

Mapping fMRI changes associated with RVT

The results obtained for the mapping of BOLD changes associated with RVT, computed from Resp and EDR, for RS, SPB and BH, are presented in Figs. 8, 9, and 10, respectively. For RS and SPB, no significant changes were found between Resp and EDR for either the number of voxels showing significant BOLD changes and the average PSC (Figs. 8 and 9, panel B). For BH, fewer voxels were associated with the EDR-derived RVT compared with Resp for the whole brain, with gray and white matter following the same pattern. No significant differences were found between Resp and HRV (Wilcoxon rank-sum test, corrected p-values). Nonetheless, the average PSC seems to be equivalent for respiration and HRV, considering either the whole brain or gray/white matter.

Discussion

We demonstrated the feasibility of extracting meaningful respiratory signals from the ECG recorded in the MRI environment for the first time. Using different methods, we compared the extracted EDR signals with the measured respiration signal, both during resting state and two respiration-modulation tasks. Overall, the HRV method, which relies on heart rate changes modulated by respiration, exhibited the best performance across tasks, explaining the BOLD-signal variance as well as measured respiration. Our results indicate that EDR holds great potential for physiological noise correction or CVR imaging, in cases when respiration cannot be recorded, or the signal is corrupted, particularly in the context of EEG-fMRI.

Similarity between EDR and measured respiration signals

In general, all EDR methods yielded similar respiratory traces to the ground-truth, when using the optimal lag, with EMD showing the highest similarity. Consistently with our results, Abreu et al. (2017) also found this method to be the most accurate for EDR estimation in the MRI environment, in terms of both temporal dynamics and spectral content[16]. Moreover, our results demonstrated high coherence values in addition to the strong correlations. Nevertheless, by comparing the EDR signals with the ground-truth respiration signals in our study, we found that correlations are generally low at a lag of 0 s, with the optimal time lag varying considerably

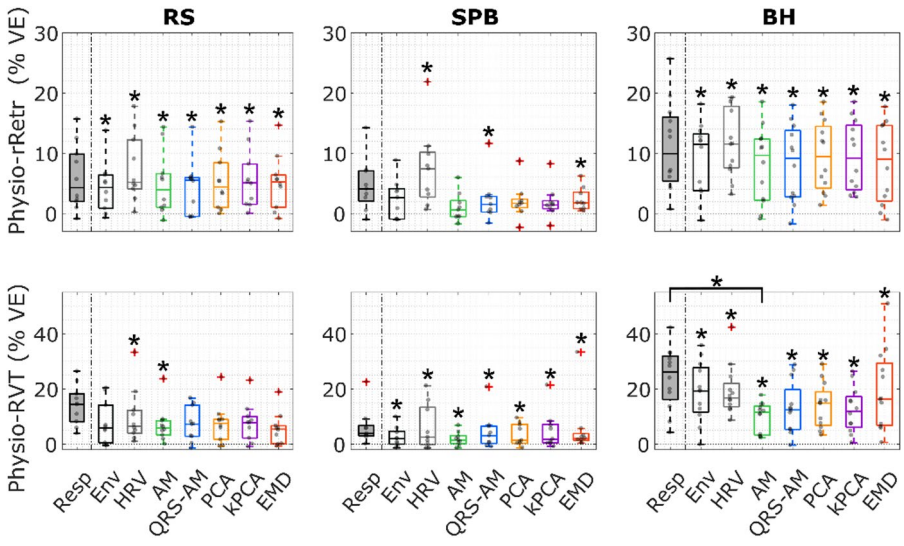

Fig. 6. Distributions across subjects of the GM average fMRI signal Variance Explained (%VE) by the respiratory regressors relative to a basic model ($VE_{Physio} - VE_{Basic}$), for Resp (gray box plot) and each EDR method (x-axis, colours): (Top) Physio-rRetr: including the RETROICOR respiratory terms; and (Bottom) Physio – RVT: includes RVT. Square brackets with * outside the plots denote significant differences between methods (Kruskal-Wallis test, corrected p-values); * inside the plots denote values significantly larger than zero for each method (Wilcoxon signed-rank test, corrected p-values). *Env* ECG Envelope, *HRV* Heart Rate Variability, *AM* Amplitude Modulation, *QRS-AM* QRS-area Modulation, *PCA* Principal Component Analysis, *kPCA* Kernel Principal Component Analysis, *EMD* Empirical Mode Decomposition.

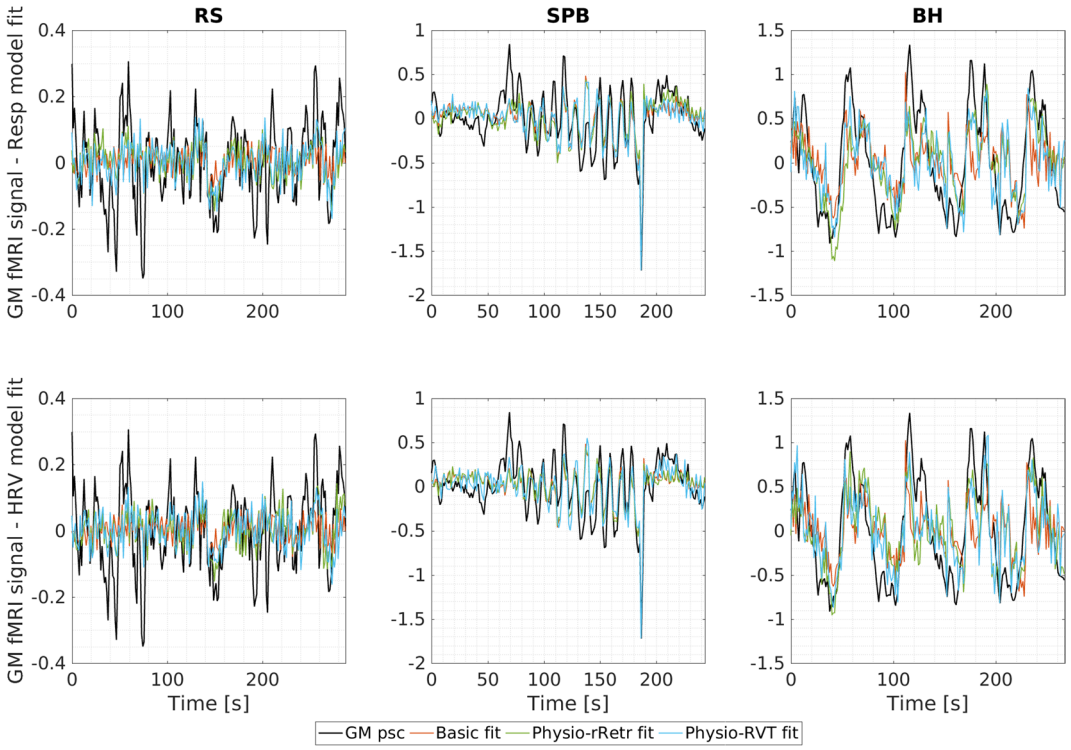

Fig. 7. GM average BOLD percent signal change in each task, for an illustrative subject: original preprocessed BOLD signal (GM PSC) and respective model fit using only basic regressors (Basic fit) and cardiac regressors adding either RETROICOR respiratory terms (Physio-rRetr fit) or RVT (Physio – RVT fit), obtained from Resp and HRV.

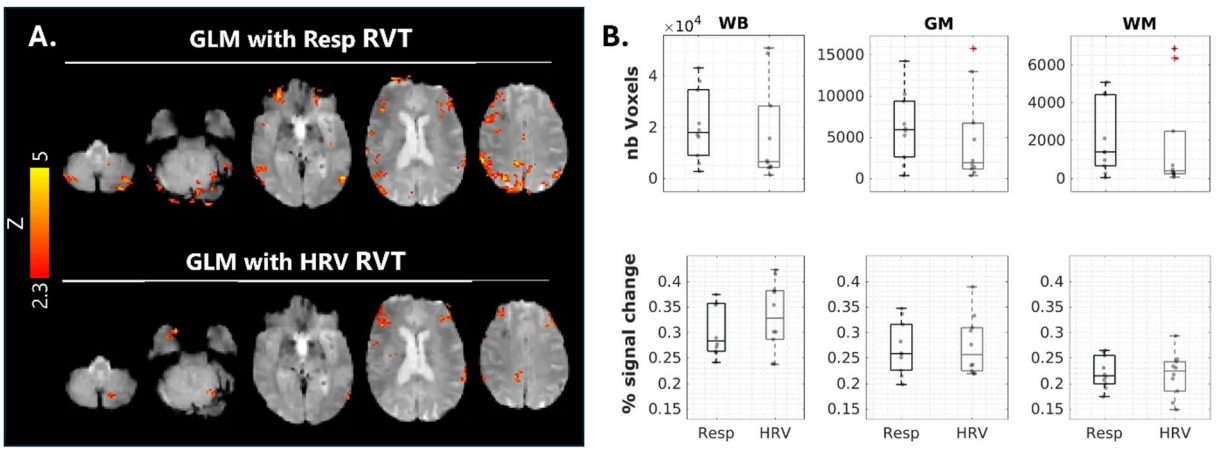

Fig. 8. Physiological noise: mapping of fMRI changes associated with RVT for RS. (**A**) Illustrative subject: map of significant BOLD modulation with RVT (z-stat map, cluster threshold 2.3; p-value < 0.05; and (**B**) Group results: distributions across subjects of volume (nb voxels, top) and average amplitude (% signal change, bottom) of significant BOLD modulation with RVT.

between subjects. In fact, none of the methods could be linked to a fixed lag based on our time lag study, which would have enabled further research to use them in situations where the respiratory signal is unavailable for retrieval. Furthermore, it may be dependent on the respiratory frequency itself, which will in principle be unknown as well. This EDR time lag dependence and variability represents a limitation when a ground-truth respiration is not available. In contrast, coherence values are unaffected by time lags, and they were high across all tasks. The HRV method exhibited the highest coherence, despite low correlation. At the other end, amplitude-based methods had the lowest coherence values, indicating their inability to effectively capture the frequency content of the measured respiration.

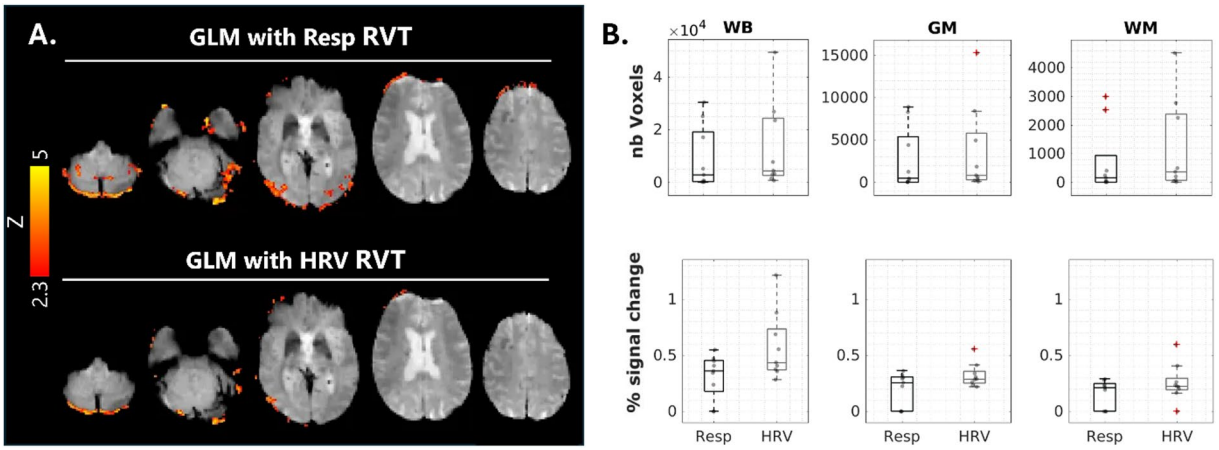

Fig. 9. Physiological noise: mapping of fMRI changes associated with RVT for SPB. (**A**) Illustrative subject: map of significant BOLD modulation with RVT (z-stat map, cluster threshold 2.3; p-value < 0.05) and (**B**) Group results: distributions across subjects of volume (nb voxels, top) and average amplitude (% signal change, bottom) of significant BOLD modulation with RVT.

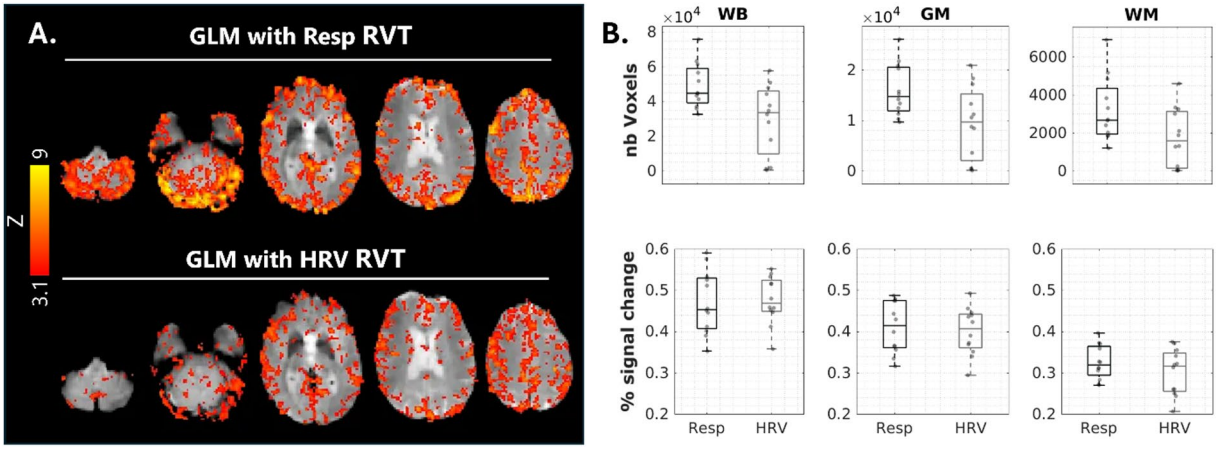

Fig. 10. CVR imaging: mapping of fMRI changes associated with RVT for BH; (**A**) Illustrative subject: map of significant BOLD modulation with RVT (z-stat map, cluster threshold 3.1; p-value < 0.05 and (**B**) Group results: distribution across subjects of volume (nb voxels) and average amplitude (% signal change) of BOLD modulation with RVT.

It is important to note that several well-established direct methods exist for measuring respiration, including respiratory belts[33], nasal temperature/airflow sensors[34], capnography[35], inductive plethysmography[36], and spirometry[37]. However, each method has limitations: nasal/oral airflow sensors can be uncomfortable for participants, may interfere with natural breathing patterns, and are sensitive to displacements or obstruction; respiratory belts may slip or shift during longer recordings, potentially introducing measurement artifacts; capnography requires a tight-fitting mask or cannula, which can be intrusive and impractical and inductive plethysmography or spirometry, while accurate, often involve additional equipment and calibration, increasing setup complexity and participant burden[38,39]. Although these methods are regarded as gold standards and are often highly accurate, their practical challenges, together with the strict need for MRI-compatibility, highlight the importance of considering alternative approaches that may be more practical and less intrusive in the MRI environment.

Our study does not aim to propose EDR as a replacement for these direct methods, but rather to demonstrate its utility as a practical surrogate in EEG-fMRI settings where direct recordings are unavailable, corrupted, or technically challenging to acquire. Within this context, the observed similarities between EDR and the measured respiration signals reinforce the potential of EDR to capture meaningful respiratory fluctuations while acknowledging its intrinsic limitations.

Physiological signal modelling in fMRI analysis

Physiological noise correction is often necessary to remove non-neuronal contributions to the BOLD signal[9]. Because frequency features play an important role in estimating physiological regressors, the high coherence of HRV signals allowed this method to provide the best models for all tasks. Additionally, the voxelwise analysis showed that HRV-based EDR also yielded BOLD signal changes associated with RVT that were similar to those obtained using the measured respiration signals, for both resting state and slow-paced breathing. These results indicate that the HRV EDR approach may be useful for the purpose of physiological noise correction when respiration is lacking. For CVR imaging based on the breath-holding task, the EDR-based model yielded similar BOLD percent signal change values compared with respiration, although with a considerably lower number of voxels activated across the whole brain and the gray matter. These results indicate that, despite being less sensitive, EDR may provide reliable CVR estimates.

Relation with the EDR literature

Although EDR methods have not previously been evaluated against the respiration ground truth using ECG signals recorded in the MR environment, a substantial literature exists for recordings conducted outside of it[38,39]. Of special relevance to our work, a few studies have investigated the performance of EDR methods in conditions with varying breathing patterns[15,40,41]. Varon et al. (2020) systematically compared several types of methods for estimating EDR, assessing respiratory wave morphology, respiratory rate and cardiorespiratory information[15]. They applied the EDR methods to three datasets with a variety of physiological conditions, including relaxation, stress and healthy/abnormal sleep patterns. Their findings showed that simple methods based on morphological changes of the ECG caused by respiration, particularly those relying on the QRS complex, outperformed the other ones. The fact that our findings are not aligned with this study, may be explained by the distortion of the ECG in the MRI environment. Even after MR-artifact correction and further preprocessing, residual artifacts inevitably persist, and the typical ECG signal morphology is not preserved. As a result, amplitude-based methods are expected to perform poorly in our case. Additionally, the placement of the ECG electrode in the EEG-fMRI setup (on the subject's back, as recommended for artifact minimization) differs from the standard single-lead ECG montage used in most EDR studies. This may further affect the waveform morphology, making direct comparisons with the literature challenging.

Machine learning, including deep learning models, have also been utilized to infer respiratory information from fMRI spatiotemporal patterns[42,43]. However, these models are more complex and require larger datasets, which makes them more difficult to apply to the typically small EEG-fMRI datasets. Furthermore, they are more challenging to implement in real time when needed.

Limitations

One of the greatest limitations of our study is the need for optimizing the lag introduced by the EDR estimation, which may hinder the use of EDR signals alone for assessing respiratory patterns at specific time points. Another limitation is the strong dependence of the EDR on the quality of the ECG data, as any degradation in ECG signal quality can significantly affect the accuracy of EDR estimations. Furthermore, it can be difficult to distinguish between cardiac and respiratory contributions when analyzing fMRI data, primarily due to the inherent nature of the EDR signal, which integrates both physiological processes. Similarly, it may be that the good performance of the HRV method is also linked to the ability to explain an autonomic system component, as this system is closely related to heart rate variability in general and may contribute to the BOLD signal.

In addition, HRV-based EDR methods require careful interpretation, since respiration does not modulate the heart rate in a single, uniform manner. For example, respiration-entrained oscillations[44,45], in which neural oscillatory activity is phase-locked to the respiratory cycle, can influence ECG-derived measures and complicate the interpretation of correlations with respiration. Likewise, both classical respiratory sinus arrhythmia (RSA) and negative RSA (nRSA) have been described. Classical RSA is characterized by heart rate acceleration during inspiration[46], while nRSA corresponds to heart rate deceleration during inspiration, and has been associated particularly with MRI-related anxiety[47–49]. These phenomena highlight that the relationship between respiration and cardiac activity is complex and context dependent. As a result, HRV-derived EDR signals should be understood as capturing correlations between respiration and cardiac activity, rather than providing evidence of a direct causal influence. Although they cannot differentiate RSA from nRSA, these signals can still serve as valid regressors for fMRI analyses provided that the underlying modulation pattern remains consistent throughout the recording. Notably, the performance of HRV-based EDR may be reduced in a minority of participants with anxiety, who often exhibit specific respiratory patterns accompanied by nRSA, potentially complicating the interpretation of correlations between respiration, cardiac activity, and BOLD signals. In our sample, at the time of scanning participants were screened for anxiety with STAI-S[50] showing a median of 31 (range = 21–42) which in local norms[51] falls within the range of absence / low anxiety (these results are not discussed further as they fall outside the scope of the present work).

Moreover, additional caution is required when using EDR for physiological noise correction. Respiration is closely coupled with brain metabolism and energetics[52], and EDR does not perfectly reflect respiration but may also capture broader cardiorespiratory influences. Consequently, indiscriminate removal of EDR-related fluctuations could eliminate physiologically meaningful BOLD signal components. For this reason, EDR should be applied with careful consideration of study aims, balancing its utility for noise modeling with its potential to provide complementary physiological information.

The variability in respiratory influences on the ECG also highlights the intrinsic richness of the respiratory signal itself, which can carry multiple distinct features and even serve as a human fingerprint[53], underscoring that EDR provides only a partial representation of respiration.

Conclusion

Our study demonstrates the feasibility of extracting respiratory signals from ECG in the MRI environment and highlights the potential of this approach even in the presence of respiratory modulations, making it useful for monitoring and the computation of physiological regressors in fMRI analysis. The HRV method showed the best performance across tasks, indicating the potential of using EDRs as a physiological regressor in EEG-fMRI studies where direct respiration data is unavailable or corrupted. Importantly, we demonstrated the performance of EDR methods, not only during resting state, but also during respiratory manipulations of slow-paced breathing and breath-holding, broadening the range of potential applications.

Data availability

Data supporting this study will be made available by the corresponding author upon reasonable request.

Received: 4 July 2025; Accepted: 3 October 2025
Published online: 11 November 2025

References

1. Birn, R. M., Diamond, J. B., Smith, M. A. & Bandettini, P. A. Separating respiratory-variation-related fluctuations from neuronal-activity-related fluctuations in fMRI. *NeuroImage* **31**, 1536–1548 (2006).
2. Birn, R. M., Smith, M. A., Jones, T. B. & Bandettini, P. A. The respiration response function: the Temporal dynamics of fMRI signal fluctuations related to changes in respiration. *NeuroImage* **40**, 644–654 (2008).
3. Chang, C., Cunningham, J. P. & Glover, G. H. Influence of heart rate on the BOLD signal: the cardiac response function. *NeuroImage* **44**, 857–869 (2009).
4. Glover, G. H., Li, T. Q. & Ress, D. Image-based method for retrospective correction of physiological motion effects in fMRI: RETROICOR. *Magn. Reson. Med. Off J. Int. Soc. Magn. Reson. Med.* **44**, 162–167 (2000).
5. Bulte, D. & Wartolowska, K. Monitoring cardiac and respiratory physiology during FMRI. *NeuroImage* **154**, 81–91 (2017).
6. Behzadi, Y., Restom, K., Liau, J. & Liu, T. T. A component based noise correction method (CompCor) for BOLD and perfusion based fMRI. *NeuroImage* **37**, 90–101 (2007).
7. Salimi-Khorshidi, G. et al. Automatic denoising of functional MRI data: combining independent component analysis and hierarchical fusion of classifiers. *NeuroImage* **90**, 449–468 (2014).
8. Pruim, R. H. R. et al. ICA-AROMA: A robust ICA-based strategy for removing motion artifacts from fMRI data. *NeuroImage* **112**, 267–277 (2015).
9. Addeh, A., Williams, R. J., Golestani, A., Pike, G. B. & MacDonald, M. E. Physiological confounds in BOLD-fMRI and their correction. *NMR Biomed.* **38**, 1–27 (2025).
10. Przystup, P., Poliński, A., Wtorek, J. Q. R. S. & Morphology-Based EDR Signal—Factors determining its properties. *IEEE Access.* **10**, 34665–34676 (2022).
11. Moody, G. B., Mark, R. G., Zoccola, A. & Mantero, S. Derivation of respiratory signals from Multi-lead ECGs. *Comput. Cardiol.* **12**, 113–116 (1985).
12. Yasuma, F. & Hayano, J. *Respiratory Sinus Arrhythmia Chest* **125**, 683–690 (2004).
13. Dong, K. et al. An integrated framework for evaluation on typical ECG-derived respiration waveform extraction and respiration. *Comput. Biol. Med.* **135**, 104593 (2021).
14. Boyle, J., Bidargaddi, N., Sarela, A. & Karunanithi, M. Automatic detection of respiration rate from ambulatory Single-Lead ECG. *IEEE Trans. Inf. Technol. Biomed.* **13**, 890–896 (2009).
15. Varon, C. et al. A comparative study of ECG-derived respiration in ambulatory monitoring using the Single-lead ECG. *Sci. Rep.* **10**, 5704 (2020).
16. Abreu, R., Nunes, S., Leal, A. & Figueiredo, P. Physiological noise correction using ECG-derived respiratory signals for enhanced mapping of spontaneous neuronal activity with simultaneous EEG-fMRI. *NeuroImage* **154**, 115–127 (2017).
17. Abreu, R., Leal, A. & Figueiredo, P. EEG-Informed fMRI: A review of data analysis methods. *Front Hum. Neurosci* **12**, (2018).
18. Niendorf, T., Winter, L. & Frauenrath, T. *In Adv. Electrocardiograms Methods Anal* (BoD – Books on Demand, 2012).
19. Pinto, J., Bright, M. G., Bulte, D. P. & Figueiredo, P. Cerebrovascular reactivity mapping without gas challenges: A methodological guide. *Front. Physiol.* **11**, 608475 (2021).
20. Domingos, C. et al. Impact of susceptibility-induced distortion correction on perfusion imaging by pCASL with a segmented 3D GRASE readout. *Magn. Reson. Imaging.* **102**, 141–150 (2023).
21. Esteves, I. et al. Uncovering longitudinal changes in the brain functional connectome along the migraine cycle: a multilevel clinical connectome fingerprinting framework. *J. Headache Pain*. **26**, 29 (2025).
22. Fouto, A. R. et al. Impact of truncating diffusion MRI scans on diffusional kurtosis imaging. *Magn. Reson. Mater. Phys. Biol. Med.* https://doi.org/10.1007/s10334-024-01153-y (2024).
23. Fouto, A. R. et al. Alterations of white matter microstructure in migraine patients vary in the peri-ictal phases. *eNeuro* ENEURO.0300-24.2024 (2024). https://doi.org/10.1523/ENEURO.0300-24.2024
24. Guadilla, I. et al. White matter alterations in episodic migraine without aura patients assessed with diffusion MRI: effect of free water correction. *J. Headache Pain*. **26**, 31 (2025).
25. Matoso, A. et al. Involvement of the cerebellum in structural connectivity enhancement in episodic migraine. *J. Headache Pain*. **25**, 154 (2024).
26. Ruiz-Tagle, A. et al. Preserved working memory performance along with subcortical modulation during peri-ictal phases in spontaneous migraine attacks. *Headache J. Head Face Pain*. **65**, 407–419 (2025).
27. Jenkinson, M., Beckmann, C. F., Behrens, T. E. J., Woolrich, M. W. & Smith, S. M. *FSL NeuroImage* **62**, 782–790 (2012).
28. Niazy, R. K., Beckmann, C. F., Iannetti, G. D., Brady, J. M. & Smith, S. M. Removal of FMRI environment artifacts from EEG data using optimal basis sets. *NeuroImage* **28**, 720–737 (2005).
29. de Chazal, P. et al. Automated processing of the single-lead electrocardiogram for the detection of obstructive sleep Apnoea. *IEEE Trans. Biomed. Eng.* **50**, 686–696 (2003).
30. Varon, C. & Van Huffel, S. ECG-derived respiration for ambulatory monitoring. in Cardiol. Conf. CinC 169–172 (IEEE, 2015). (2015). https://doi.org/10.1109/CIC.2015.7408613
31. Widjaja, D., Varon, C., Dorado, A., Suykens, J. A. K. & Van Huffel, S. Application of kernel principal component analysis for Single-Lead-ECG-Derived respiration. *IEEE Trans. Biomed. Eng.* **59**, 1169–1176 (2012).
32. Zvolanek, K. M. et al. Comparing end-tidal CO2, respiration volume per time (RVT), and average Gray matter signal for mapping cerebrovascular reactivity amplitude and delay with breath-hold task BOLD fMRI. *NeuroImage* **272**, 120038 (2023).
33. Seppänen, T. M., Alho, O. P. & Seppänen, T. Reducing the airflow waveform distortions from breathing style and body position with improved calibration of respiratory effort belts. *Biomed. Eng. OnLine*. **12**, 97 (2013).

34. Patel, R., Gireesan, K., Sengottuvel, S., Janawadkar, M. P. & Radhakrishnan, T. S. Suppression of baseline wander artifact in magnetocardiogram using breathing sensor. *J. Med. Biol. Eng.* **37**, 554–560 (2017).
35. Kerslake, I. & Kelly, F. Uses of capnography in the critical care unit. *BJA Educ.* **17**, 178–183 (2017).
36. Sackner, M. A. et al. Calibration of respiratory inductive plethysmograph during natural breathing. *J. Appl. Physiol. Bethesda Md.* **1985 66**, 410–420 (1989).
37. Miller, M. R. et al. Standardisation of spirometry. *Eur. Respir J.* **26**, 319–338 (2005).
38. Liu, H., Allen, J., Zheng, D. & Chen, F. Recent development of respiratory rate measurement technologies. *Physiol. Meas.* **40**, 07TR01 (2019).
39. Vitazkova, D. et al. Advances in respiratory monitoring: A comprehensive review of wearable and remote technologies. *Biosensors* **14**, 90 (2024).
40. Orphanides, G. A., Karittevlis, C., Alsadder, L. & Ioannides, A. A. Using spectral continuity to extract breathing rate from heart rate and its applications in sleep physiology. *Front. Physiol.* **15**, 1446868 (2024).
41. Sharma, H. & Sharma, K. K. Sleep apnea detection from ECG using variational mode decomposition. *Biomed. Phys. Eng. Express.* **6**, 015026 (2020).
42. Bayrak, R. G., Salas, J. A., Huo, Y. & Chang, C. A. Deep pattern recognition approach for inferring respiratory volume fluctuations from fMRI data. in Med. Image Comput. Comput. Assist. Interv. – MICCAI 2020 (ed (eds Martel, A. L. et al.) 428–436 (Springer International Publishing, doi:https://doi.org/10.1007/978-3-030-59728-3_42 (2020).
43. Addeh, A. et al. Direct machine learning reconstruction of respiratory variation waveforms from resting state fMRI data in a pediatric population. *NeuroImage* **269**, 119904 (2023).
44. Goheen, J. et al. Dynamic mechanisms that couple the brain and breathing to the external environment. *Commun. Biol.* **7**, 938 (2024).
45. Zelano, C. et al. Nasal respiration entrains human limbic oscillations and modulates cognitive function. *J. Neurosci.* **36**, 12448–12467 (2016).
46. Yasuma, F. & Hayano, J. Respiratory sinus arrhythmia: why does the heartbeat synchronize with respiratory rhythm? *Chest* **125**, 683–690 (2004).
47. Pfurtscheller, G., Rassler, B., Schwarz, G. & Klimesch, W. Scan-associated anxiety (scanxiety): the enigma of emotional breathing oscillations at 0.32 Hz (19 bpm). *Front Neurosci* **18**, (2024).
48. Rassler, B., Schwerdtfeger, A., Aigner, C. S. & Pfurtscheller, G. Switch-Off of respiratory sinus arrhythmia can occur in a minority of subjects during functional magnetic resonance imaging (fMRI). *Front Physiol* **9**, (2018).
49. Rassler, B., Blinowska, K., Kaminski, M. & Pfurtscheller, G. Analysis of respiratory sinus arrhythmia and directed information flow between brain and body indicate different management strategies of fMRI-Related anxiety. *Biomedicines* **11**, 1028 (2023).
50. Spielberger, C. D., Gorsuch, R. L., Lushene, R., Vagg, P. R. & Jacobs, G. A. *Manual for the State-Trait Anxiety Inventory (Form Y)* (Consulting Psychologists, 1983).
51. Silva, D. R. & Campos, R. Alguns Dados normativos do Inventário de Estado-Traço de Ansiedade – Forma Y (STAI-Y), de Spielberger, Para a população Portuguesa. *Rev. Port Psicol.* **33**, 71–89 (1998).
52. Goheen, J., Anderson, J. A. E., Zhang, J. & Northoff, G. From lung to brain: respiration modulates neural and mental activity. *Neurosci. Bull.* **39**, 1577–1590 (2023).
53. Soroka, T. et al. Humans have nasal respiratory fingerprints. *Curr. Biol.* **35**, 3011–3021e3 (2025).

Author contributions

IE: Methodology, Software, Formal analysis, Investigation, Data Curation, Writing – original draft, Writing – review and editing, Visualization; ARF: Investigation, Resources, Data Curation; ART: Investigation, Resources, Data Curation; GC: Investigation, Resources, Writing – review and editing; PF: Methodology, Conceptualization, Resources, Writing – review and editing, Supervision, Project administration, Funding acquisition. All authors have approved the final manuscript.

Funding

This work was supported by LARSyS FCT funding [DOI: https://doi.org/10.54499/LA/P/0083/2020, https://doi.org/10.54499/UIDP/50009/2020, and https://doi.org/10.54499/UIDB/50009/2020], PRR project Center for Responsible AI [grant C645008882-00000055] and FCT [grants PD/BD/150356/2019, PTDC/EMD-EMD/29675/2017, LISBOA-01-0145-FEDER-029675].

Declarations

Competing interests

The authors declare no competing interests.

Additional information

Supplementary Information The online version contains supplementary material available at https://doi.org/10.1038/s41598-025-23131-7.

Correspondence and requests for materials should be addressed to I.E.